Appl. Phys. A (2005)
DOI: 10.1007/s00339-005-3343-9

Applied Physics A
Materials Science & Processing

M. ROHMER✉
C. WIEMANN
M. MUNZINGER
L. GUO
M. AESCHLIMANN
M. BAUER

Local correlation of photoemission electron microscopy and STM at a defined cluster substrate system

Department of Physics, University of Kaiserslautern, Erwin-Schrödingerstr. 46, 67663 Kaiserslautern, Germany

Received: 9 February 2005/Accepted: 6 July 2005
© Springer-Verlag 2005

ABSTRACT We describe a technique that enables photoelectron spectroscopy and STM imaging of supported clusters from identical surface areas of a size of a few μm^2 at a lateral resolution in the low nanometer regime. In this way we are able to locally correlate properties regarding the electronic structure of the clusters and their topography. The use of a photoemission electron microscope (PEEM) allows one to probe the local distribution of the photoemission yield. An STM-tip is used to remove clusters from their position and set local, well-defined markers at the surface that are clearly visible in the PEEM images. These markers act as reference points to identify surface areas in the PEEM image that have formerly been imaged by an STM. The present accuracy of this local correlation technique is at least 300 nm. We propose a scheme to further improve this correlation so that in future experiments even selected single clusters, which have been characterized by STM, can be addressed by local photoelectron spectroscopy as well as local time-resolved photoelectron spectroscopy.

PACS 73.22.Lp; 79.60.Jv; 61.46.+w

1 Introduction

Conventional photoelectron spectroscopy (PES) and related photoemission techniques have been widely used in the past to characterize the electronic structure of clusters supported by a substrate [1–4]. Despite the undisputed and important contribution of PES, e.g., to a better understanding of cluster–substrate interactions, the significance of these results is generally restricted by the lateral integration over a macroscopic area [5, 6], even if complementary techniques, such as scanning probe microscopy, have been used for a representative (however in any case lateral only selective) characterization of the surface and cluster topography on a nanometer scale. It is, for example, often difficult to definitely exclude a residual uncertainty of the photoemission data with respect to the actual origin of the signal. A considerable contribution to the photoemission yield can arise, e.g., from the supporting surface or surface defects. In view of these problems an experimental approach that allows local photoelectron spectroscopy of selected areas, which have been previously characterized by STM, is desirable. Using the technique of photoemission electron microscopy (PEEM), local photoelectron-spectroscopy from selected surface areas is possible with a lateral resolution down to the sub-10 nm regime [7–9]. Just recently, several groups successfully applied this technique in the study of cluster surface systems [10–12]. It is, therefore, ideally suited to be combined with high resolution STM, which gives the required complementary information about e.g., cluster distribution and cluster topography.

In this paper we present the realization of a locally correlated photoemission and STM experiment. Our approach enables us to perform photoemission spectroscopy and STM imaging of supported clusters from identical areas of the surface down to sizes of about 1 μm^2 and below. In this way, a definite correlation of the photoemission signal to a surface area completely characterized by STM is possible.

The outline of the paper is the following: After a short description of the experimental setup, we will discuss some details regarding the preparation and the properties of the cluster–substrate system – Ag/HOPG – chosen for our investigations. We will first describe the general experimental challenges that have to be solved to achieve a local correlation between the photoemission signal and the STM. The detailed procedure chosen to achieve this goal for the Ag/HOPG system is then presented. In the final discussion and outlook, we will briefly discuss the relevant conclusions that can be drawn from the presented local correlation experiment.

2 Experimental

2.1 *Experimental setup*

The experimental setup consists of an ultrahigh-vacuum chamber for sample preparation, STM and PEEM imaging, and a tunable femtosecond Ti:sapphire laser system. A schematic view of the experimental setup is shown in Fig. 1. For sample preparation, the chamber is equipped with a commercial sputter gun (50–5000 eV kinetic energy), an e-beam heating stage (up to 1450 K) and a Knudsen cell-type evaporation source combined with a quartz thickness monitor. At the main chamber, photoemission imaging is done by a commercial PEEM instrument (Focus IS-PEEM) as described in [13]. The microscope is mounted in a μ-metal chamber to shield external stray magnetic fields that would affect the imaging quality of the system with respect to the

✉ Fax: +49 631 205 3903, E-mail: rohmer@physik.uni-kl.de

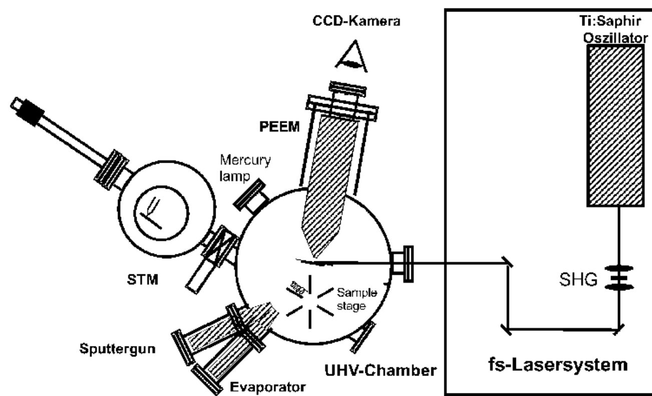

FIGURE 1 Scheme of the experimental setup

lateral resolution. The resolution that we achieved at a reference sample (periodic palladium structures at silicon) was 40 nm with a 10/90 criteria at a step. Point structures can be separated for distances ≥ 20 nm [7]. Note, however, that in general the surface under investigation has to be considered as part of the PEEM-optics and that, therefore, the imaging quality and resolution can be affected by the surface properties [14]. As well as measuring the local distribution of the overall electron yield emitted from the surface, local electron spectroscopy can be performed with the setup by using a MicroESCA system ($\Delta E \approx 80$ meV, $\Delta x \approx 1$ μm) or a retarding field analyzer (RFA) mounted in front of the imaging PEEM detector ($\Delta E \approx 200$ meV, $\Delta x \approx 20$ nm). Attached to the main chamber is a commercial UHV-STM (Park Scientific Instruments) that allows characterization of the surface topography with a maximum scan field of $10 \times 10\,\mu m^2$ and at this scan size with a resolution of about 5 Å. Sample transfer between both systems is performed in-situ. Two different light sources can be used to record PEEM images: a conventional mercury vapor UV source (energy cut-off at 4.9 eV) and a tunable femtosecond Ti:sapphire laser system (80 MHz rep. rate, 120 fs pulse width, wavelength tunable between 750–850 nm) frequency doubled in a 0.2-mm-thick beta barium borate (BBO) crystal to produce blue light at $h\nu$ 2.9–3.3 eV. Using the UV source, the lateral distribution of regular one-photon photoemission (1PPE) close to threshold emission is imaged by the PEEM. In the case of the pulsed femtosecond laser system, the high peak intensities of the output lead to nonlinear photoemission by means of multi-photon absorption. For the present experiments, the ultra short laser pulses are focused onto the sample so that sufficiently high intensities are achieved to induce two-photon photoemission.

2.2 *Sample Preparation*

The well-defined cluster–surface system chosen for these investigations has been studied in detail before by means of STM, UPS and 2PPE [2, 4, 5, 15]. This particular system provides reasonable referencing of our measurements to experimental data obtained with well established techniques. The sample was prepared following a procedure described in detail in [5, 16]. The graphite sample was tape cleaved in air, then annealed in UHV at pressures lower than 10^{-8} mbar at 600 °C for about one hour and finally at 1000 °C

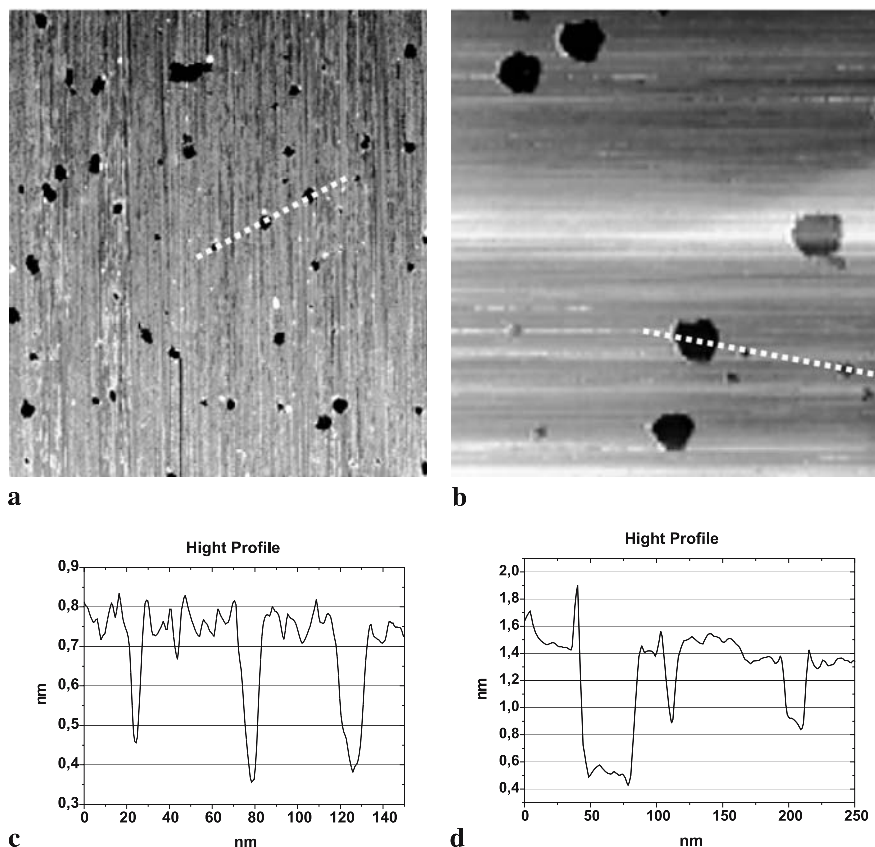

FIGURE 2 (**a**) $400 \times 400\,nm^2$ STM image of a HOPG-substrate sputtered with 100 eV Argon ions after 8 min oxidation at 560 °C and (**b**) according line scan. (**c**) $400 \times 400\,nm^2$ STM image of a HOPG-substrate sputtered with 1000 eV Argon ions after 20 min oxidation at 530 °C and (**d**) according line scan. A substrate preparation using Argon sputtering energies of 1 keV leads to vacancy defects in the HOPG at a depth of up to four monolayers. After oxidation, the deeper holes dominate the fraction of the surface (see (**b**)) due to their higher oxidation rates. After reduction of the ion energy to 100 eV, exclusively 1 ML deep pits are found after the oxidation (see (**d**)). The size and depth distribution of the pits is in qualitative agreement with the common reference [17]

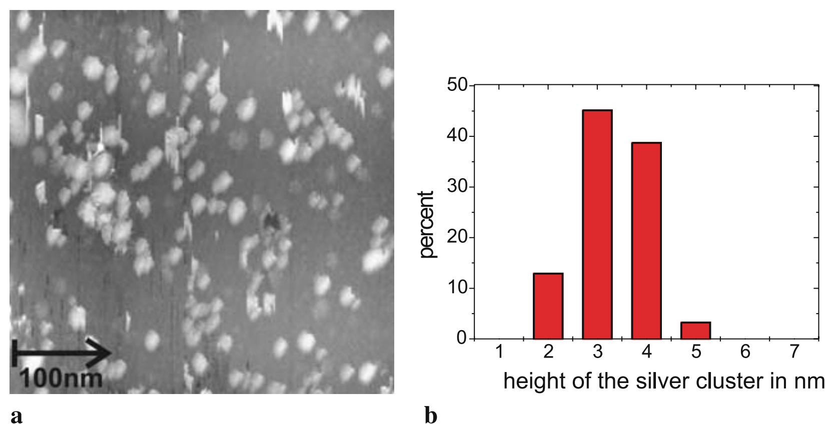

FIGURE 3 (**a**) $400 \times 400\,\mathrm{nm}^2$ STM image of the surface shown in Fig. 2 (**b**) after evaporation of 1 ML of silver. The cluster density is $625\,\mathrm{cluster}/\mu\mathrm{m}^2$, corresponding to a mean distance of the clusters of 40 nm. (**b**) measured height distribution of the silver clusters in figure (**a**)

for a few minutes. STM images of the HOPG after this procedure showed a flat surface over extended areas, separated by steps and a negligible defect density, as typically observed for these systems. In the next step, the graphite was argon-sputtered for 20 seconds at 100 eV kinetic energy to create one mono-layer (1ML) deep vacancy defects (VD), which act as a point of attack for oxygen in the subsequent oxidation step. The use of a low kinetic energy for the sputtering procedure is motivated by detailed studies by Hahn and Kang [17] and significantly improved the homogeneity of the final hole distribution (see Fig. 2a,b) in comparison to an earlier publication of our work [11]. The so-prepared sample was oxidized at 560 °C in air for 8 min and the vacancy defects (VD) were expanded by the oxidation to 3–10 nm holes. After annealing in vacuum, 1 ML of silver was evaporated at room temperature at a deposition rate of 0.4 ML/min resulting in the condensation of silver clusters in the holes at a defined and narrow size distribution [5, 16]. Figure 3a shows an STM scan (0.3 V gap voltage, 0.1 nA tunnel current) of the final sample state. In order to assure constant-current mode of the STM and to minimize the influence of the STM tip to the sample, a low scan-speed of 50 nm/s was chosen. Advanced scanning with these parameters over a longer period shows that the tip does not influence the cluster distribution. The shape of the so-formed clusters is slightly oblate at a height to diameter ratio of 0.7, independent of cluster size [16]. The diameter can, therefore, be directly inferred from the measured cluster height. The visible lateral extension of the cluster in the STM scan can only be regarded as an upper limit of the actual diameter; for objects of this size, the tip diameter and shape significantly contribute to the signal [5]. For the present sample we find an average cluster height of 3.5 nm corresponding to a diameter of 5 nm. The size distribution is rather narrow, in correspondence to reference literature [16, 18]], and is displayed in Fig. 3b as represented by the height distribution. The cluster density of the sample is determined to $625\,\mathrm{cluster}/\mu\mathrm{m}^2$, corresponding to a mean distance between two clusters of about 40 nm.

3 Experimental results

3.1 *Local correlation of* PEEM *and* STM

Figure 4 shows a high resolution PEEM image (field of view = $7 \times 7\,\mu\mathrm{m}^2$) of the HOPG surface, after cluster condensation, recorded in the 2PPE modus using the short-pulse laser source. The clear structuring of the photoemission yield distribution is in contrast to the homogenous and low yield observed for an uncovered (but sputtered and etched) HOPG surface. Moreover, the photoemission yield from single areas of the silver covered substrate exceeds that of the pure HOPG by a factor of about 50. The structure in the PEEM image reflects properties of the silver cluster distribution at the HOPG surface (see also detailed discussion in [11]). However, the visible structure density in the PEEM image is significantly reduced in comparison to the actual cluster density at the surface as determined by STM (see Fig. 3 and note the different length scales in image 3 and image 4). For the present case we find that the cluster density exceeds the structure density of the photoemission distribution by a factor of about 20. This deviation is in qualitative agreement with an earlier PEEM investigation of Ag-clusters on HOPG prepared under slightly different conditions [11]. In the latter work we interpreted the reduced density in the PEEM images in terms of a distinctive selectivity of the 2PPE process to specific cluster properties. Although we made extensive use of the degrees of freedom of the experimental setup as offered by the laser source (polarization, tunability in laser wavelength), the observed results did not allow us to identify these properties. We have already suggested in this earlier work that an enhanced, high local correlation of STM and PEEM images is necessary to specify the origin of this selectivity. Therefore, a useful experimental approach has to be found that enables a complete

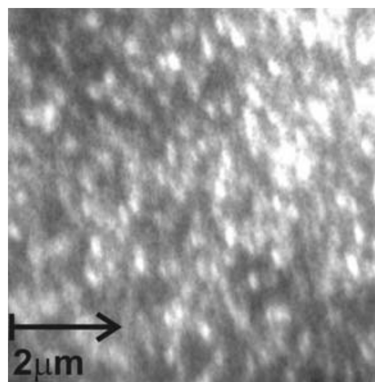

FIGURE 4 A $7 \times 7\,\mu\mathrm{m}^2$ large area of the cluster covered surface imaged by PEEM in the 2PPE modus

lateral characterization and identification of identical areas by PEEM and STM.

In the experimental setup, STM and PEEM are separate imaging components and a sample transfer has to be performed in order to apply both microscopy techniques to image the surface. After a transfer process from the STM sample holder to the PEEM sample holder any information about the absolute position of the STM scan field(s) at the surface will be lost. Therefore, to locate an area in a PEEM image that has been previously topographically characterized by STM, a local reference feature or marker within the scan area is required that can be unambiguously identified by the STM as well as by the PEEM. The lateral signal distribution from the silver clusters is not a suitable characteristic as it appears too homogeneous for both imaging techniques and also differs significantly in its appearance between STM and PEEM, as described above.

The use of unique and pronounced surface defects, particularly intersecting large steps (height bigger than 20 nm), which can be clearly identified in STM and PEEM, is in principle possible but rather impractical for the present system for the following reasons. These defects appear in general rather arbitrarily and – at least for a well prepared HOPG-substrate – at a length scale of a tenth of a millimeter. The typically restricted scan area of STM (maximum 10 by 10 μm^2 for the used system) generally requires multiple attempts to find a sample area exhibiting such a feature. Furthermore, for typical studies of cluster substrate systems (local) sample conditions should be defined as well as possible; one in general intends to avoid experimental studies nearby such substantial substrate modifications.

A more sophisticated and satisfactory approach would be, if the reference marker to be identified could be purposely placed at the surface. This would considerably reduce the accidental nature of such a correlation experiment. It is the potential of the STM-tip to manipulate the surface topography which can be used to realize such an approach. The main task is to make sure that such a STM-marker can be read out, by identifying it with the PEEM. A potential scheme for a PEEM-STM correlation experiment can then be performed as follows:

In a first step, an area of interest is scanned and characterized by the STM. After a successful scan, a marker (size about a few μm^2) is set by the tip at a defined distance with respect to this scanned area. This is possible because of the highly accurate and reproducible positioning performance of the STM scanner and because of the capability of the tip to sweep the silver cluster out of the scanned area using adequate scan parameters [11, 16]. According to the large difference of the photoemission yield between pure HOPG and silver-covered HOPG, especially in the 2PPE-mode, these cleaned areas are visible as dark rectangles even in PEEM images of a rather large field of view (PEEM overview mode: field of view is about $\sim 500\,\mu m$). It is possible to span a coordinate system in the relevant region by multi markers as, e.g., shown in Fig. 5.

After the transfer of the sample plate into the PEEM, the surface is imaged in the overview mode and moved by the sample coarse position system until the markers are relocated at the PEEM image. This can be done with passable expense.

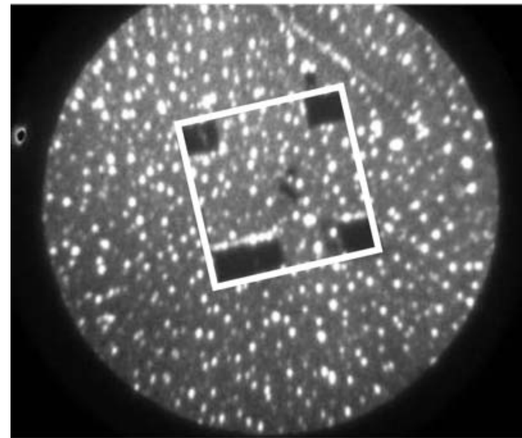

FIGURE 5 2PPE-PEEM ($h\nu = 3.1$ eV) image of an Ag/HOPG surface with distinct markers set by the STM. This image shows an HOPG-substrate that was Argon sputtered at 1 keV, oxidized for 20 min at 530 °C and covered with 0.5 ML silver. The field of view is about 30 μm in diameter. At the corners of the maximum scan range of the STM ($10 \times 10\,\mu m$), three $2 \times 2\,\mu m^2$ and one $2 \times 4\,\mu m^2$ big markers are visible. The white rectangle indicates the maximum possible scan range of the STM scanner

The next step is to zoom into the marked area and identify the location of the sector previously characterized by STM using the set reference markers visible in the PEEM image. This allows a distinct and highly local correlation of the STM image and high resolution PEEM.

Figure 6b is a striking example of the capability of STM to set the required markers to be identified in the PEEM image. It shows a $14.5 \times 13\,\mu m^2$ cut out of an PEEM image where we can recognize a $9 \times 9\,\mu m^2$ area and a interleaved $3 \times 3\,\mu m^2$ area where the photoemission yield is significantly lower than in the surrounding region. In this areas the sample surface was destructively scanned and "marked" by STM scans with high bias-voltages (about 3 V), high tunneling currents (around 1.5 nA), high scan-speed and low feedback loop. According to this scanning in constant-height-mode, the STM tip moved all silver particles out of the scanned area leaving a clean HOPG surface. Figure 6a is the STM scan of the $9 \times 9\,\mu m^2$ big area after removal of the silver cluster showing the topography of the underlying HOPG substrate. Characteristic points at the image are marked. The circles A and D mark scratches at the surface and the circle C the crossing of a scratch and HOPG step of about 30 nm height (see also B). These points are also marked in the PEEM image in Fig. 6b. As expected for a clean HOPG surface, the swept area shows negligible photoemission, and only topographic structures, such as scratches and steps, deliver a significant photoemission yield. In contrast, the silver-covered surrounding areas which have not been modified by the STM give rise to a strong uniform photoemission yield modulated by the topographic contrast.

An example of a defined coordinate system set in this way and imaged with the PEEM is shown in Fig. 5. At the corners of the maximum STM scan range, markers of different size have been placed. The allocation of a non-destructive STM scan relative to this marker can be done with an accuracy higher than 300 nm. The white rectangular in Fig. 5 indicates the maximum scan area of the STM.

Figure 7 shows an example of a local correlation of an area within a PEEM-image and an imaging STM scan of a clus-

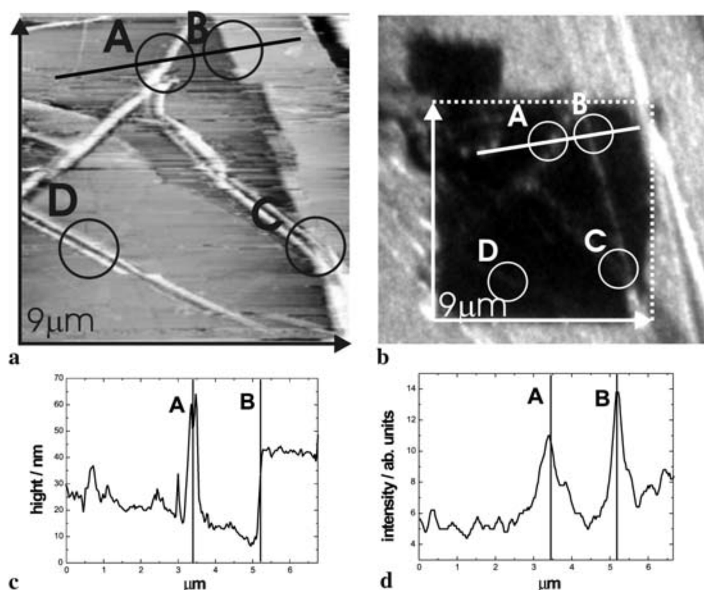

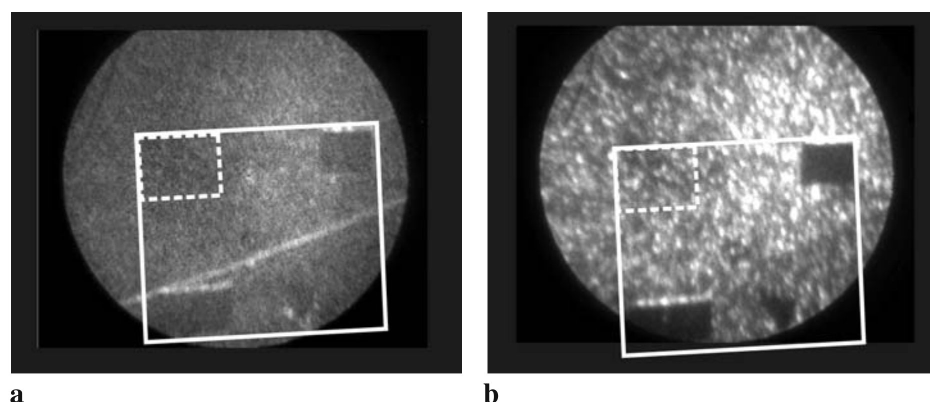

FIGURE 6 (**a**) Topographic STM image ($9 \times 9\,\mu m^2$) recorded after a destructive STM scan where the silver clusters had been swept away from the area. (**b**) Sector of an PEEM image comprising the scanned area shown in figure (**a**). The used excitation source is a conventional mercury vapor UV source (energy cut-off at 4.9 eV). (**c**) Line scan drawn in the STM image. (**d**) Line scan drawn in the PEEM image. In both images the *circles* A and D mark scratches at the surface, B marks an ca. 30 nm high HOPG step and C the crossing of a scratch with this step. The characteristic substrate defect structure in this area is clearly visible in the STM and PEEM image

a b

FIGURE 7 PEEM images recorded in 1PPE (**a**) and 2PPE (**b**) modus. In both images the white rectangular outlines the $10 \times 10\,\mu m^2$ wide area, that can be scanned and manipulated by the STM. The dot rectangle located at the left top corner marks the area where the cluster decorated HOPG has been imaged by the STM. Both rectangles correspond to square areas which are horizontally distorted by about 15% due to aberration of the PEEM optics at large magnification

ter covered HOPG area realized in this way. The STM scan ($3 \times 3\,\mu m^2$) has been performed in the upper left corner of the maximum area that can be covered with the scanner. The corresponding image (Fig. 8a) shows that this area is exclusively decorated with well separated clusters with a diameter of 3–5 nm and a cluster density of 625 cluster/μm^2. Each dot in the STM image corresponds to a cluster. No other topographic structure is visible in this field. Due to the relatively large area to be scanned, a slow scanning rate had to be chosen to avoid destruction of the clusters; therefore, a single scan takes about 25 min. To prove that this scan did not result in destruction of the surface, it was imaged several times. No change in the cluster decoration and topography could be observed. After this imaging procedure, two markers of different size were set with the STM tip at opposite corners of the maximal scanner range, below and to the right of the imaged field. To locate these markers in the PEEM image after sample transfer we used the above-described procedure. After detection of the markers, a photoemission image of the relevant area was taken. The corresponding PEEM images of this sample area are shown in Fig. 8b and c. The markers, where the Ag-Cluster had been removed by the STM tip, appear dark in the 1PPE PEEM image (Fig. 7a) as well as in the 2PPE image (Fig. 7b) and are clearly distinguishable from the non-scanned areas. Note that at the top border of these fields an enhanced PE contrast is observed, visible in Fig. 7a and b particularly in the left bottom rectangle. It is a result of the accumulation of silver that had been removed by the STM-tip from the scanned area. The chosen corner position of these markers with respect to the maximum scan range of the STM enables us to reconstruct the maximum possible field of view of the STM in the PEEM image. The white rectangle in Fig. 7a and b indicates this $10 \times 10\,\mu m^2$ large area.

These two markers and their well-known relative position with respect to the maximum scan field allow one to locate the area that has been imaged by the STM in the PEEM images in an unambiguous way. This area is marked in Fig. 7a and b by the white dotted rectangle located at the upper left corner. For better comparison, we display the 1PPE-PEEM and 2PPE-PEEM signal distribution from the marked area scaled to the size of the corresponding STM image in Fig. 8a, b and c. To our knowledge, this figure represents the first direct correlation of the lateral photoemission distribution and the topography of supported clusters from identical surface areas.

3.2 *Discussion and outlook*

The main purpose of this paper was to describe an experimental approach that allows a high local correlation of

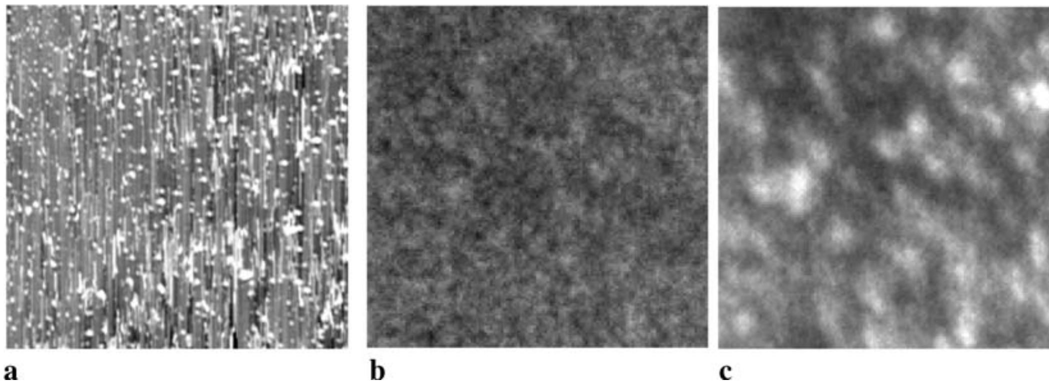

FIGURE 8 STM (**a**), 1PPE (**b**), and 2PPE (**c**) image of an identical surface area of the cluster covered HOPG marked in Fig. 7 by the white dotted rectangular (size: $3 \times 3\ \mu m^2$). For the 2PPE image we find, in comparison to the 1PPE image and the STM scan, a structure density reduced by about a factor of twenty. The STM scan showd interferences in scan direction (here vertical) due to the extreme scan parameters necessary to perform a non destructive scanning of the relatively large area. Even though the lateral resolution is somewhat reduced, the measured height of all visible dots is between 2 to 4 nm, in correspondence with the measured cluster height distribution (Fig. 3). Every feature represents a single silver cluster or a few close-lying silver clusters

photoemission and STM data from a cluster–surface system. Figure 7 and 8 show that this is indeed possible by making use of the surface-manipulating capabilities of the STM-tip. The STM, 1PPE and 2PPE images shown in Fig. 8a, b and c respectively, contain complementary information about the clusters from an identical area at the surface. Statements about cluster density and the homogeneity of the cluster system with respect to shape and size can be made from the STM image. We find by STM imaging that this area is covered with well separated clusters, with sizes ranging from 3–5 nm and density of 625 cluster/μm^2 corresponding to a mean distance of about 40 nm. The actual size of the clusters lies obviously beyond the lateral resolution of the PEEM. Considering the mean distance between two clusters which lies in the range of the PEEM resolution, the cluster should appear as separable spots in the PEEM image. This is indeed the case for the 1PPE PEEM image; a clear structuring is visible resembling the cluster density as determined from the STM scan. Due to the uncertainty in the local correlation between STM and PEEM image of 300 nm and due to the statistic distribution of the cluster decoration, an unambiguous identification of identical local structures in the STM and PEEM image is not possible for the present sample.

The lateral intensity distribution of the conventional 1PPE-PEEM image reflects local properties related to the electronic density of states in the initial and final state of the photoemission process as well as local variations in the cluster and substrate work function. The 2PPE-PEEM images are additionally affected by the coupling of the exciting laser light ($h\nu \approx 3.1$ eV) to localized collective plasmon excitations of the silver clusters ($\hbar\omega \approx 3.0$–3.6 eV) [11, 18] and the involvement of single electron excitations in the 2PPE process which are located between Fermi energy and vacuum level [19]. The visible differences between the 2PPE images and the 1PPE and STM image, respectively, in the lateral signal distribution can be related to these specific properties. The significant difference in structure density between the 2PPE image and the STM image has been mentioned before and was already discussed in some detail in [11]. The local correlation of the PEEM image and the STM scan unambiguously shows that this difference is intrinsic to small clusters exhibiting a rather narrow size distribution.

The selectivity of the 2PPE process appears to be highly sensitive to very small differences in the cluster properties with respect to their topography (see cluster height distribution in Fig. 3). Plasmon resonance energy and resonance width, however, can be strongly modified by only relatively small changes in the cluster shape, the cluster size and the cluster–substrate coupling [20, 21]. In this regard, it is intuitive that 2PPE particularly address clusters exhibiting a plasmon energy in resonance with the chosen photon energy of 3.1 eV. 'Off-resonant' clusters stay hidden in a 2PPE image. The signal distribution visible in the 1PPE-image (Fig. 8a) supports this conclusion. The 1PPE process ($h\nu \approx 4.9$ eV) cannot be affected by selective coupling of the light to the plasmon resonance. In consequence, the structure density appears much denser in comparison to the 2PPE image, and is compatible with the cluster density in the STM image.

It is obvious that the achieved correlation of PEEM and STM is a first and important step to match our photoemission and topographic results. However, more quantitative statements require further improvement of the local correlation between PEEM and STM. Although e.g., effects due to local variations in the cluster density are possible, they cannot be considered in detail at the present state. It seems that it is first necessary to relate a specific photoemission feature to a selected cluster characterized by the STM (single cluster spectroscopy). This can be achieved for samples with smaller cluster densities so that identical structure signatures can be identified in the STM and the PEEM image at the same time. An alternate approach would involve the use of a pattern recognition algorithm. Highly local spectroscopy of plasmon excitations, and highly local 1 photon and 2 photon photoemission spectroscopy can also be performed with the used PEEM system, and will be able to complement these experiments. Most exciting, however, is the capability of 2PPE (2PPE-PEEM) to be combined with femtosecond pump–probe spectroscopy (time-resolved 2PPE) [22]. This technique allows one to measure the decay dynamics of electronic excitations at a resolution in the femtosecond regime. In combination with the presented approach, experiments will be possible addressing the femtosecond decay dynamics in single clusters, in which size and location will have been previously probed on a nanometer scale by STM.

4 Summary

An experimental scheme has been realized that allows a complete characterization of identical surface areas of a cluster–substrate system by means of local photoemission spectroscopy using photoemission electron microscopy (PEEM) and STM. The local correlation achieved so far is better than 300 nm for an area size of $3 \times 3\ \mu m^2$. We assume that the use of low density cluster systems and pattern recognition schemes will significantly improve this correlation by an accuracy of several nanometers. In future experiments we plan to use the potential of this technique to perform highly local femtosecond pump–probe photoemission of deposited clusters which are well-characterized on a nanometer scale.

ACKNOWLEDGEMENTS Special thanks go to H. Hövel and W. Pfeiffer for helpful suggestions regarding the preparation of the sample. This work was supported by the Deutsche Forschungsgemeinschaft through SPP 1153.

REFERENCES

1 G.K. Wertheim, S.B. DiCenzo, S.E. Youngquist: Phys. Rev. Lett. **51**, 2310 (1983); M.G. Mason: Phys. Rev. B **27**, 748 (1983); S.L. Qiu, X. Pan, M. Strongin, P.H. Citrin: Phys. Rev. B **36**, 1292 (1987); H.-V. Roy, P. Fyet, F. Patthey, W.-D. Schneider, B. Delley, C. Massobrio: Phys. Rev. B **49**, 5611 (1994)
2 H. Hövel, B. Grimm, M. Pollmann, B. Reihl: Phys. Rev. Lett. **81**, 4608 (1998)
3 U. Busolt, E. Cottancin, H. Röhr, L. Socaciu, T. Leisner, L. Wöste: Appl. Phys. B **68**, 453 (1999)
4 J. Lehmann, M. Merschdorf, W. Pfeiffer, A. Thon, S. Voll, G. Gerber: Phys. Rev. Lett. **85**, 2921 (2000)
5 H. Hövel: Appl. Phys. A **72** 295 (2001)
6 K.-H. Meiwes-Broer: In: *Metal Clusters at Surfaces*, K.-H. Meiwes-Broer (ed.), Springer, Berlin (2000), pp. 151–174
7 C. Ziethen, O. Schmidt, G.H. Fecher, C.M. Schneider, G. Schönhense, R. Frömter, M. Seider, K. Grzelakowski, M. Merkel, D. Funnemann, W. Swiech, H. Gundlach, J. Kirschner: J. Electron. Spectrosc. Related Phenom. **88–91**, 983 (1998)
8 H. Ade, W. Yang, S.L. English, J. Hartman, R.F. Davis, R.J. Nemanic: Surf. Rev. Lett. **5**, 1257 (1998)
9 T. Schmidt, S. Heun, J. Slezak, J. Diaz, K.C. Prince: Surf. Rev. Lett. **5**, 1287 (1998)
10 M. Cincetti, A. Oelsner, G.H. Fecher, H.J. Elmers, G. Schönhense: Appl. Phys. Lett. **83**, 1503 (2003)
11 M. Munzinger, C. Wiemann, M. Rohmer, L. Guo, M. Aeschlimann, M. Bauer: New J. Phys. **7**, 1 (2005)
12 J. Rockenberger, F. Nolting, J. Lüning, J. Hu, P. Alivisatos: J. Chem. Phys. **116**, 6322 (2002)
13 W. Swiech, G.H. Fecher, C. Ziethen, O. Schmidt, G. Schönhense, K. Grzelakowski, C.M. Schneider, R. Frömter, H.P. Oepen, J. Kirschner: J. Elec. Spec. Rel. Phenom. **84**, 171 (1997)
14 S.A. Nepijko, N.N. Sadov, G. Schöhense, M. Escher, X. Bao, W. Huang, Ann. Phys. (Leipzig) **9**, 441 (2000)
15 M. Merschdorf, C. Kennerknecht, K. Willig, W. Pfeiffer: New J. Phys. **4**, 95 (2002)
16 H. Hövel, T. Becker, A. Bettac, B. Reihl, M. Tschudy, E.J. Williams: J. Appl. Phys. **81**, 154 (1997)
17 J.R. Hahn, H. Kang, S.M. Lee, Y.H. Lee: J. Phys. Chem. B **103** (1999); J.R. Hahn, H. Kang: Phys. Rev. B **60**, 8 (1999); J.R. Hahn, H. Kang: Surf. Sci. Lett. **446** (2000); J.R. Hahn, H. Kang: J. Phys. Chem. B **106** (2002)
18 M. Merschdorf, W. Pfeiffer, A. Thon, S. Voll, G. Gerber: Appl. Phys. A **71**, 547 (2000)
19 For an overview on Two Photon Photoelectronspectroscopy and is application to different systems see e.g. T. Fauster, W. Steinmann: In: *Photonic Probes of Surfaces*, P. Halevi (ed.), *Electromagnetic Waves: Recent Developments in Research* Vol. **2**, North-Holland, Amsterdam (1995), pp. 347–411
20 J. Tiggesbäumer, L. Köller, K.H. Meiwes-Broer, A. Liebsch: Phys. Rev. A **48**, R17 490 (1993)
21 N. Nilius, N. Ernst, H.-J. Freund: Phys. Rev. Lett. **84**, 3994 (2000)
22 O. Schmidt, M. Bauer, C. Wiemann, R. Porath, M. Scharte, O. Andreyev, G. Schönhense, M. Aeschlimann: Appl. Phys. B **74**, 3 (2002)